Advances in Applied Mathematics and Mechanics
Adv. Appl. Math. Mech., Vol. **18**, No. 1, pp. 109-133

DOI: 10.4208/aamm.OA-2023-0325
February 2026

Fully Discrete Schemes with First- and Second-Order Temporal Accuracy for the Incompressible Magnetohydrodynamic Flow Based on the Generalized Scalar Auxiliary Variable Approach

Huimin Ma and Pengzhan Huang*

College of Mathematics and System Sciences, Xinjiang University, Urumqi, Xinjiang 830017, China

Received 20 December 2023; Accepted (in revised version) 21 August 2024

Abstract. Based on the generalized scalar auxiliary variable approach and vector penalty projection method, some fully discrete schemes with first- and second-order accuracy in time direction are constructed for solving the incompressible magnetohydrodynamic model. It is a combination of mixed finite element approximation for spatial discretization and first-order backward Euler/second-order backward differential formula for temporal discretization. The proposed schemes own several features: it decouples unknown physical variables and linearizes the nonlinear terms, then it only needs to solve some linear equations at each temporal level; although the divergence of numerical velocity is not exactly equal to zero, it can approximately meet the mass conservation when one takes small penalty parameter; while the computation of the velocity and pressure are decoupled, numerical results show that the velocity and pressure can reach second-order accuracy in time. The resulting schemes are supported by numerical analysis and simulation.

AMS subject classifications: 65M60, 65M12

Key words: Magnetohydrodynamic model, stability analysis, generalized scalar auxiliary variable, vector penalty projection.

1 Introduction

The incompressible magnetohydrodynamic (MHD) model, which is comprised of the incompressible Navier-Stokes equations and the Maxwell equations via Lorentz force and

*Corresponding author.
Emails: huiminmhm@163.com (H. Ma), hpzh@xju.edu.cn (P. Huang)

Ohm's law, is commonly used to describe the interaction between a viscous, incompressible, electrically conducting fluid and an external magnetic field. It has important applications in fusion technology, submarine propulsion system, liquid metals in magnetic pumps and so on [13,18,42].

In this paper, we consider the following time-dependent MHD equations. Given a bounded and regular domain $\Omega\subset\mathbb{R}^d$, $d=2$ or 3, and for a final time $T>0$, find the velocity field $\mathbf{u}:(0,T]\times\Omega\to\mathbb{R}^d$, the pressure $p:(0,T]\times\Omega\to\mathbb{R}$ and the magnetic field $\mathbf{H}:(0,T]\times\Omega\to\mathbb{R}^d$ satisfying [21,42]

$$\mathbf{u}_t-\nu\Delta\mathbf{u}+\nabla p=\mathbf{f}-(\mathbf{u}\cdot\nabla)\mathbf{u}-\mu\mathbf{H}\times\mathrm{curl}\mathbf{H} \quad \text{in } \Omega\times(0,T], \tag{1.1a}$$

$$\mathrm{div}\mathbf{u}=0 \quad \text{in } \Omega\times(0,T], \tag{1.1b}$$

$$\mu\mathbf{H}_t+\sigma^{-1}\mathrm{curlcurl}\mathbf{H}=\sigma^{-1}\mathrm{curl}\mathbf{g}+\mu\mathrm{curl}(\mathbf{u}\times\mathbf{H}) \quad \text{in } \Omega\times(0,T], \tag{1.1c}$$

$$\mathrm{div}\mathbf{H}=0 \quad \text{in } \Omega\times(0,T], \tag{1.1d}$$

with initial data and homogeneous boundary condition

$$\mathbf{u}(\mathbf{x},0)=\mathbf{u}_0(\mathbf{x}),\quad \mathbf{H}(\mathbf{x},0)=\mathbf{H}_0(\mathbf{x}) \quad \text{with } \mathrm{div}\mathbf{u}_0=0,\quad \mathrm{div}\mathbf{H}_0=0 \quad \text{in } \Omega, \tag{1.2a}$$

$$\mathbf{u}|_{S_T}=0,\quad \mathbf{H}\cdot\mathbf{n}|_{S_T}=0,\quad \mathbf{n}\times\mathrm{curl}\mathbf{H}|_{S_T}=0, \tag{1.2b}$$

where $S_T:=\partial\Omega\times[0,T]$ and $\mathbf{n}$ represents the unit outward normal of the boundary $\partial\Omega$. The model has three physical parameters: ν is the kinematic viscosity, μ is the magnetic permeability and σ is the electric conductivity. The vector-value functions $\mathbf{g}$ and $\mathbf{f}$ represent the known applied current satisfying $(\mathbf{n}\times\mathbf{g})|_{S_T}=0$ and the external force, respectively.

Numerical approximation of the MHD model is challenging, because it is a system with nonlinear terms, coupling of multi-physics fields and divergence-free. Faced with those challenges, researchers have designed a series of efficient numerical schemes by applying the finite element method [17, 64], finite difference method [8, 12], finite volume method [10,45], Fourier spectral method [19] for spatial discretization and the first-order Euler semi-implicit scheme [17, 22, 63, 65], the first-order Euler implicit/explicit scheme [59], Crank-Nicolson scheme [15, 24, 39, 51, 69], second-order backward differential formula [34, 60, 74], projection type scheme [20, 46, 52, 62, 71, 72], time filter scheme [11, 25], blended backward differential formula scheme [36, 37], deferred correction scheme [16] and so on. One of the challenges in numerically solving the MHD equations is the treatment of nonlinear terms, which can be divided into several types: fully implicit, semi-implicit and explicit schemes. It is known that when the convection and Lorentz force terms are treated by fully implicit and semi-implicit schemes, the velocity and magnetic field are not completely decoupled, which will increase the computational complexity. Compared to the above schemes, the explicit scheme [38, 44, 59] can decouple the velocity and magnetic field at each time step. Then the computational scale and the storage times of matrix are reduced. Usually, it is conditionally stable. Furthermore, Zhang et al. [66, 67] proposed first-order fully decoupled scheme, which is unconditionally energy stable.

Recently, the scalar auxiliary variable (SAV) method, which was introduced by Shen et al. [47–49] for gradient flow models, has attracted considerable attention due to its superiority to preserve unconditional energy stability. The idea of the SAV method has developed into a powerful way to design some unconditionally energy stable numerical schemes for various complex nonlinear systems, such as the Navier-Stokes equation [32,35,75], Schrödinger equation [4], and Cahn-Hilliard-Navier-Stokes equations [30] and so on. In addition, researchers have developed this idea to the MHD model. Based on an auxiliary variable associated with the total system energy function, Zhang and Yang [73] constructed a decoupled, linearized finite element scheme with first-order time accuracy and established the unconditional stability and optimal error estimates. To address the theoretical and practical issues from the nonlinear algebraic equation in [35,73], Li et al. [33] proposed a new auxiliary variable, which was initially introduced in [32] for the Navier-Stokes equations. Furthermore, inspired by the idea of "zero-energy-contribution" (introduced by Yang in [54–58]), a fully discrete finite element scheme with second-order time accuracy has been presented for solving the MHD model by Zhang et al. [68] and Yang et al. [61]. After that, Wang [50] introduced two novel schemes that combined the SAV method with the pressure-correction method, and proposed three adaptive time-stepping strategies. Carter et al. [6] developed two unconditionally stable, linear ensemble algorithms, in which the nonlinear terms were discretized by fully explicit scheme under the generalized positive auxiliary variable approach and the artificial viscosity stabilization. Based on the exponential SAV approach, Chen et al. [7] constructed first- and second-order schemes for the MHD model with variable density and derived a rigorous error analysis for the first-order scheme.

Later, with the in-depth study of researchers, the generalized SAV approach is proposed for more general dissipative systems [9, 26–28, 53]. Compared with the original SAV method, the generalized SAV only requires solving one decoupled linear system with constant coefficients at each time step and is also unconditionally energy stable. Li et al. [31] proposed a linear, unconditionally stable first-order semi-discrete scheme for the Navier-Stokes equations, which combined the generalized SAV scheme with the consistent splitting method. The authors carried out global error estimates in 2D case as well as local error estimates in 3D case for velocity and pressure. Then, based on the generalized SAV approach, a variable time-step IMEX-BDF2 scheme for the Navier-Stokes equation with periodic boundary conditions was proposed by Di et al. [14]. Zhang et al. [70] combined the relaxation technique [29] and the generalized SAV method to solve the gradient flow, which enjoyed all advantages of the generalized SAV approach and dissipated modified energy that was directly linked to the original free energy.

The objective of this paper is to develop some fully discrete, stable finite element schemes with first- and second-order accuracy in time for the time-dependent incompressible MHD model, and ensure that one gets control of mass conservation law for the discrete solution. The latter will be implemented by using the vector penalty projection (VPP_ε) method, which is proposed by Angot et al. [1–3] and extended to the time-dependent incompressible MHD model [41]. Motivated by the idea provided in [2, 53],

we first introduce an equivalent system of the time-dependent incompressible MHD model (1.1a)-(1.2b). Then, based on the generalized SAV and VPP$_\varepsilon$ method, we present first- and second-order fully discrete schemes, which meet the requirement of full decoupling and only need to solve a sequence of linear equations with constant coefficient at each time step. Moreover, the stability of the proposed schemes is established. To the best of the authors' knowledge, it is the first work which obtains the stability of the fully discrete VPP$_\varepsilon$ scheme. Some numerical experiments are provided to demonstrate the effectiveness of the proposed schemes.

An outline of this paper is as follows. Some notations, function spaces and the equivalent form of the considered model are introduced in Section 2. In Section 3, we construct first- and second-order fully discrete schemes and obtain stability of the proposed schemes. Several numerical simulations and comparisons with the existing scheme demonstrate the performance of the proposed schemes in the last section.

2 Preliminaries

Throughout the paper, we will need some notations and preliminary lemma which are used frequently. For $m\in\mathbb{N}^+$ and $1\le p\le\infty$, the usually Sobolev space $W^{m,p}(\Omega)$ is equipped with the norm $\|\cdot\|_{W^{m,p}(\Omega)}$. For $m=0$, $L^p(\Omega)=W^{0,p}(\Omega)$ and its norm is denoted by $\|\cdot\|_{L^p(\Omega)}$. For $p=2$, $H^m(\Omega)=W^{m,2}(\Omega)$ with the norm $\|\cdot\|_m$. In addition, $\|\cdot\|_0$ and $(\cdot,\cdot)$ denote the $L^2(\Omega)$ norm and its inner product on the domain Ω. For the MHD model (1.1a)-(1.2b), the natural function spaces are introduced:

$$\mathbf{X}=\{\mathbf{v}\in H^1(\Omega)^d:\mathbf{v}|_{\partial\Omega}=0\},\quad M=\{q\in L^2(\Omega):(1,q)=0\},$$
$$\mathbf{W}=\{\mathbf{B}\in L^2(\Omega)^d,\,\mathrm{curl}\mathbf{B}\in L^2(\Omega)^d:\mathbf{B}\times\mathbf{n}|_{\partial\Omega}=0\}.$$

With the above definitions of the function spaces, the corresponding variational formulation of the model (1.1a)-(1.2b) reads as: find $(\mathbf{u},p,\mathbf{H})\in\mathbf{X}\times M\times\mathbf{W}$, for all $(\mathbf{v},q,\mathbf{B})\in\mathbf{X}\times M\times\mathbf{W}$ and $t\in(0,T]$ such that [22]

$$(\mathbf{u}_t,\mathbf{v})+\nu(\nabla\mathbf{u},\nabla\mathbf{v})+((\mathbf{u}\cdot\nabla)\mathbf{u},\mathbf{v})+\mu(\mathbf{H}\times\mathrm{curl}\mathbf{H},\mathbf{v})-(\mathrm{div}\mathbf{v},p)=(\mathbf{f},\mathbf{v}),\tag{2.1a}$$
$$\mu(\mathbf{H}_t,\mathbf{B})+\sigma^{-1}(\mathrm{curl}\mathbf{H},\mathrm{curl}\mathbf{B})-\mu(\mathbf{u}\times\mathbf{H},\mathrm{curl}\mathbf{B})=\sigma^{-1}(\mathbf{g},\mathrm{curl}\mathbf{B}),\tag{2.1b}$$
$$(\mathrm{div}\mathbf{u},q)=0,\tag{2.1c}$$
$$\mathbf{u}(\mathbf{x},0)=\mathbf{u}_0(\mathbf{x}),\mathbf{H}(\mathbf{x},0)=\mathbf{H}_0(\mathbf{x}).\tag{2.1d}$$

Next, we introduce an equivalent form for the MHD equations based on the idea of [53]. Taking the L^2 inner product of $\mathbf{u}$, p and $\mathbf{H}$ with (1.1a), (1.1b) and (1.1c), respectively, we obtain

$$\frac{1}{2}\frac{\mathrm{d}}{\mathrm{d}t}\|\mathbf{u}\|_0^2+\nu\|\nabla\mathbf{u}\|_0^2+((\mathbf{u}\cdot\nabla)\mathbf{u},\mathbf{u})+\mu(\mathbf{H}\times\mathrm{curl}\mathbf{H},\mathbf{u})=(\mathbf{f},\mathbf{u}),\tag{2.2a}$$
$$\frac{\mu}{2}\frac{\mathrm{d}}{\mathrm{d}t}\|\mathbf{H}\|_0^2+\sigma^{-1}\|\mathrm{curl}\mathbf{H}\|_0^2-\mu(\mathbf{u}\times\mathbf{H},\mathrm{curl}\mathbf{H})=\sigma^{-1}(\mathrm{curl}\mathbf{g},\mathbf{H}).\tag{2.2b}$$

By combining (2.2a) and (2.2b), we obtain the following energy law

$$\frac{1}{2}\frac{\mathrm{d}}{\mathrm{d}t}\left(\|\mathbf{u}\|_0^2+\mu\|\mathbf{H}\|_0^2\right)=-\nu\|\nabla\mathbf{u}\|_0^2-\sigma^{-1}\|\mathrm{curl}\mathbf{H}\|_0^2+(\mathbf{f},\mathbf{u})+\sigma^{-1}(\mathrm{curl}\mathbf{g},\mathbf{H}), \tag{2.3}$$

where we have used two identities

$$((\mathbf{u}\cdot\nabla)\mathbf{u},\mathbf{u})=0 \quad \text{and} \quad (\mathbf{u}\times\mathbf{H},\mathrm{curl}\mathbf{H})=(\mathbf{H}\times\mathrm{curl}\mathbf{H},\mathbf{u}).$$

Then, we introduce a scalar auxiliary variable $Q(t)=E(\mathbf{u},\mathbf{H})+C_0$, where $C_0\geq 1$ is an artificial parameter and $E(\mathbf{u},\mathbf{H}):=\frac{1}{2}\left(\|\mathbf{u}\|_0^2+\mu\|\mathbf{H}\|_0^2\right)$. Hence, according to (2.3), the original equations (1.1a)-(1.1d) are expanded as:

$$\mathbf{u}_t-\nu\Delta\mathbf{u}+(\mathbf{u}\cdot\nabla)\mathbf{u}+\mu\mathbf{H}\times\mathrm{curl}\mathbf{H}+\nabla p=\mathbf{f}, \quad \mathrm{div}\mathbf{u}=0, \tag{2.4a}$$

$$\mu\mathbf{H}_t+\sigma^{-1}\mathrm{curlcurl}\mathbf{H}-\mu\mathrm{curl}(\mathbf{u}\times\mathbf{H})=\sigma^{-1}\mathrm{curl}\mathbf{g}, \tag{2.4b}$$

$$\frac{\mathrm{d}Q}{\mathrm{d}t}=\frac{Q(t)}{E(\mathbf{u},\mathbf{H})+C_0}\Big((\mathbf{f},\mathbf{u})+\sigma^{-1}(\mathrm{curl}\mathbf{g},\mathbf{H})-\nu\|\nabla\mathbf{u}\|_0^2-\sigma^{-1}\|\mathrm{curl}\mathbf{H}\|_0^2\Big). \tag{2.4c}$$

In the last part of the section, we recall the discrete Grönwall's lemma in [23].

Lemma 2.1. *Let k, a_n, b_n and d_n for integers $n_1\leq n\leq m$ be nonnegative numbers such that*

$$a_m+k\sum_{n=n_1}^{m}b_n\leq k\sum_{n=n_1}^{m}a_nd_n+c, \quad \forall m\geq n_1.$$

Then, under the assumption $kd_n<1$, there holds

$$a_m+k\sum_{n=n_1}^{m}b_n\leq\exp\left(k\sum_{n=n_1}^{m}d_n\right)c, \quad \forall m\geq n_1.$$

3 Fully discrete schemes for the MHD model

In this section, based on the finite element approximation of the equivalent form (2.4a)-(2.4c) for the MHD model, we construct some fully discrete schemes with first- and second-order accuracy.

We introduce a spatial discretization of the MHD model (2.4a)-(2.4c) with initial data and homogeneous boundary condition (1.2a)-(1.2b) by using the mixed finite element method. From now on, let π_h be a regular, quasi-uniform triangulation of the bounded regular domain Ω into triangular K in 2D domain or tetrahedrons K in 3D case with diameters bounded by a real positive parameter $h=\max_{K\in\pi_h}\{\mathrm{diam}(K)\}$.

In below, we use Nédélec's first family of space (cf. [44]) for the unknown $\mathbf{H}$. We define

$$\mathcal{N}_1(K)=P_0(K)^d\oplus\mathcal{D}_1(K),$$

where $\mathcal{D}_1(K)$ denotes the homogeneous polynomials $\mathbf{q}(\mathbf{x})$ of degree 1 that satisfy $\mathbf{q}(\mathbf{x})\cdot\mathbf{x}=0$ on $K\in\pi_h$, and $P_k(K)$ is the set of polynomials of degree at most $k\geq 0$ on K. Additionally, we choose MINI element (cf. [5,22,61]) for the unknowns $\mathbf{u}$ and p. Consider then

$$\begin{aligned}
\mathbf{W}_h&=\{\mathbf{B}_h\in\mathbf{W}:\mathbf{B}_h|_K\in\mathcal{N}_1(K),\ \forall K\in\pi_h\},\\
\mathbf{X}_h&=\{\mathbf{v}_h\in C^0(\Omega)^d\cap\mathbf{X}:\mathbf{v}_h|_K\in(P_1(K)\oplus\text{span}\{\hat{b}\})^d,\ \forall K\in\pi_h\},\\
M_h&=\{q_h\in C^0(\Omega)\cap M:q_h|_K\in P_1(K),\ \forall K\in\pi_h\},
\end{aligned}$$

where $\hat{b}(x)\in H_0^1(K)$ takes the value 1 at the barycenter of K and such that $0\leq\hat{b}(x)\leq 1$ [5].

Moreover, let $\{t_n\}_{n=0}^N$ $(N>0)$ be a uniform partition of $[0,T]$ with time step $\Delta t=\frac{T}{N}$. Next, $(\mathbf{u}_h^n,p_h^n,\mathbf{H}_h^n)$ denote the fully discrete approximation to the solution $(\mathbf{u}(t_n),p(t_n),\mathbf{H}(t_n))$ of the problem (2.4a)-(2.4b) at $t=t_n$ and Q^n for $Q(t_n)$ in (2.4c). Besides, we set $\mathbf{f}^n=\mathbf{f}(t_n)$, and $\mathbf{g}^n=\mathbf{g}(t_n)$.

Now, based on the generalized SAV approach, we propose fully discrete VPP$_\varepsilon$ scheme with first-order accuracy in time for the equivalent system (2.4a)-(2.4c) of the incompressible MHD model.

Algorithm 3.1.

Step I: Given $\mathbf{u}_h^n,\hat{\mathbf{u}}_h^n\in\mathbf{X}_h$, $\mathbf{H}_h^n,\tilde{\mathbf{H}}_h^n\in\mathbf{W}_h$, $p_h^n\in M_h$ with $0\leq n\leq N-1$, find $(\tilde{\mathbf{u}}_h^{n+1},\tilde{\mathbf{H}}_h^{n+1})\in\mathbf{X}_h\times\mathbf{W}_h$ satisfying: for all $\mathbf{v}_h\in\mathbf{X}_h$, $\mathbf{B}_h\in\mathbf{W}_h$,

$$\begin{aligned}
&\frac{1}{\Delta t}\left(\tilde{\mathbf{u}}_h^{n+1}-\hat{\mathbf{u}}_h^n,\mathbf{v}_h\right)+\nu(\nabla\tilde{\mathbf{u}}_h^{n+1},\nabla\mathbf{v}_h)+((\mathbf{u}_h^n\cdot\nabla)\mathbf{u}_h^n,\mathbf{v}_h)+\mu(\mathbf{H}_h^n\times\text{curl}\mathbf{H}_h^n,\mathbf{v}_h)\\
&\quad-(\text{div}\mathbf{v}_h,p_h^n)=(\mathbf{f}^{n+1},\mathbf{v}_h),
\end{aligned}\tag{3.1a}$$

$$\begin{aligned}
&\frac{\mu}{\Delta t}\left(\tilde{\mathbf{H}}_h^{n+1}-\tilde{\mathbf{H}}_h^n,\mathbf{B}_h\right)+\sigma^{-1}(\text{curl}\tilde{\mathbf{H}}_h^{n+1},\text{curl}\mathbf{B}_h)-\mu(\text{curl}\mathbf{H}_h^n\times\mathbf{B}_h,\mathbf{u}_h^n)\\
&=\sigma^{-1}(\text{curl}\mathbf{g}^{n+1},\mathbf{B}_h).
\end{aligned}\tag{3.1b}$$

Step II: Based on $\tilde{\mathbf{u}}_h^{n+1}$ from (3.1a), find $\bar{\mathbf{u}}_h^{n+1}\in\mathbf{X}_h$ satisfying: for all $\mathbf{v}_h\in\mathbf{X}_h$,

$$\frac{1}{\Delta t}\left(\bar{\mathbf{u}}_h^{n+1},\mathbf{v}_h\right)+\nu(\nabla\bar{\mathbf{u}}_h^{n+1},\nabla\mathbf{v}_h)+\frac{1}{\varepsilon}\left(\text{div}\bar{\mathbf{u}}_h^{n+1},\text{div}\mathbf{v}_h\right)=-\frac{1}{\varepsilon}\left(\text{div}\tilde{\mathbf{u}}_h^{n+1},\text{div}\mathbf{v}_h\right),\tag{3.2}$$

where $0<\varepsilon\leq 1$ is a penalty parameter.

Step III: According to Step I and Step II, we get $\hat{\mathbf{u}}_h^{n+1}\in\mathbf{X}_h$ and find $p_h^{n+1}\in M_h$ by

$$\hat{\mathbf{u}}_h^{n+1}=\tilde{\mathbf{u}}_h^{n+1}+\bar{\mathbf{u}}_h^{n+1},\tag{3.3a}$$

$$(p_h^{n+1},q_h)=(p_h^n,q_h)-\frac{1}{\varepsilon}(\nabla\cdot\hat{\mathbf{u}}_h^{n+1},q_h),\quad\forall q_h\in M_h.\tag{3.3b}$$

Step IV: Given Q^n, $\hat{\mathbf{u}}_h^{n+1}$ and $\tilde{\mathbf{H}}_h^{n+1}$, compute Q^{n+1} and update the eventual velocity field $\mathbf{u}_h^{n+1}$ and magnetic field $\mathbf{H}_h^{n+1}$ by

$$\frac{Q^{n+1}-Q^n}{\Delta t}=\frac{Q^{n+1}}{E(\hat{\mathbf{u}}_h^{n+1},\tilde{\mathbf{H}}_h^{n+1})+C_0}\Big((\mathbf{f}^{n+1},\hat{\mathbf{u}}_h^{n+1})+\sigma^{-1}(\mathrm{curl}\mathbf{g}^{n+1},\tilde{\mathbf{H}}_h^{n+1}) -\nu\|\nabla\hat{\mathbf{u}}_h^{n+1}\|_0^2-\sigma^{-1}\|\mathrm{curl}\tilde{\mathbf{H}}_h^{n+1}\|_0^2\Big), \tag{3.4a}$$

$$\mathbf{u}_h^{n+1}=\gamma^{n+1}\hat{\mathbf{u}}_h^{n+1},\quad \mathbf{H}_h^{n+1}=\gamma^{n+1}\tilde{\mathbf{H}}_h^{n+1}, \tag{3.4b}$$

where

$$\gamma^{n+1}=1-\left(1-\frac{Q^{n+1}}{E(\hat{\mathbf{u}}_h^{n+1},\tilde{\mathbf{H}}_h^{n+1})+C_0}\right)^2.$$

Remark 3.1. For the above algorithm, the numerical velocity field $\mathbf{u}_h^0$,$\hat{\mathbf{u}}_h^0$ and magnetic field $\mathbf{H}_h^0$, $\tilde{\mathbf{H}}_h^0$ are needed. Here, we find $\mathbf{u}_h^0$ and $\mathbf{H}_h^0$ satisfying for all $\mathbf{v}_h\in\mathbf{X}_h$ and $\mathbf{B}_h\in\mathbf{W}_h$

$$(\nabla\mathbf{u}_h^0,\nabla\mathbf{v}_h)=(\nabla\mathbf{u}_0,\nabla\mathbf{v}_h),\quad (\mathrm{curl}\mathbf{H}_h^0,\mathrm{curl}\mathbf{B}_h)=(\mathrm{curl}\mathbf{H}_0,\mathrm{curl}\mathbf{B}_h),$$

and set

$$\hat{\mathbf{u}}_h^0=\mathbf{u}_h^0,\quad \tilde{\mathbf{H}}_h^0=\mathbf{H}_h^0,\quad Q^0=\frac{1}{2}\left(\|\mathbf{u}_h^0\|_0^2+\mu\|\mathbf{H}_h^0\|_0^2\right)+C_0,$$

which implies $Q^0>0$.

Next, we propose the second-order scheme based on backward differential formula for temporal discretization. Denote $D(s_h^n)=2s_h^n-s_h^{n-1}$, $s=p$, $\mathbf{H}$ or $\mathbf{u}$ as the second-order extrapolation of numerical approximation.

Then, based on the generalized SAV approach, we propose a fully discrete VPP$_\varepsilon$ scheme with second-order accuracy in time for the equivalent system (2.4a)-(2.4c) of the incompressible MHD model.

Algorithm 3.2.

Step I: Compute Algorithm 3.1 with $n=0$ and set $\bar{\mathbf{u}}_h^0=\mathbf{0}$.

Step II: Given $\mathbf{u}_h^{n-1},\mathbf{u}_h^n,\tilde{\mathbf{u}}_h^{n-1},\tilde{\mathbf{u}}_h^n\in\mathbf{X}_h$, $\mathbf{H}_h^{n-1},\mathbf{H}_h^n,\tilde{\mathbf{H}}_h^{n-1},\tilde{\mathbf{H}}_h^n\in\mathbf{W}_h$, $p_h^{n-1},p_h^n\in M_h$ with $1\le n\le N-1$, find $\tilde{\mathbf{u}}_h^{n+1}\in\mathbf{X}_h$ and $\tilde{\mathbf{H}}_h^{n+1}\in\mathbf{W}_h$ satisfying: for all $\mathbf{v}_h\in\mathbf{X}_h$, $\mathbf{B}_h\in\mathbf{W}_h$,

$$\frac{1}{2\Delta t}\left(3\tilde{\mathbf{u}}_h^{n+1}-4\tilde{\mathbf{u}}_h^n+\tilde{\mathbf{u}}_h^{n-1},\mathbf{v}_h\right)+\nu(\nabla\tilde{\mathbf{u}}_h^{n+1},\nabla\mathbf{v}_h)+\left((D(\mathbf{u}_h^n)\cdot\nabla)D(\mathbf{u}_h^n),\mathbf{v}_h\right) +\mu\left(D(\mathbf{H}_h^n)\times\mathrm{curl}D(\mathbf{H}_h^n),\mathbf{v}_h\right)-(\mathrm{div}\mathbf{v}_h,D(p_h^n))=(\mathbf{f}^{n+1},\mathbf{v}_h), \tag{3.5a}$$

$$\frac{\mu}{2\Delta t}\left(3\tilde{\mathbf{H}}_h^{n+1}-4\tilde{\mathbf{H}}_h^n+\tilde{\mathbf{H}}_h^{n-1},\mathbf{B}_h\right)+\sigma^{-1}(\mathrm{curl}\tilde{\mathbf{H}}_h^{n+1},\mathrm{curl}\mathbf{B}_h)-\mu\left(\mathrm{curl}D(\mathbf{H}_h^n)\times\mathbf{B}_h,D(\mathbf{u}_h^n)\right) =\sigma^{-1}(\mathrm{curl}\mathbf{g}^{n+1},\mathbf{B}_h). \tag{3.5b}$$

Step III: Based on $\tilde{\mathbf{u}}_h^{n+1}$ from (3.5a), $\bar{\mathbf{u}}_h^n$ and $\bar{\mathbf{u}}_h^{n-1}$, find $\bar{\mathbf{u}}_h^{n+1}\in\mathbf{X}_h$ satisfying: for all $\mathbf{v}_h\in\mathbf{X}_h$,

$$\begin{aligned}&\frac{1}{2\Delta t}\left(3\bar{\mathbf{u}}_h^{n+1}-4\bar{\mathbf{u}}_h^n+\bar{\mathbf{u}}_h^{n-1},\mathbf{v}_h\right)+\nu(\nabla\bar{\mathbf{u}}_h^{n+1},\nabla\mathbf{v}_h)+\frac{1}{\varepsilon}\left(\mathrm{div}\bar{\mathbf{u}}_h^{n+1},\mathrm{div}\mathbf{v}_h\right)\\&=-\frac{1}{\varepsilon}\left(\mathrm{div}\tilde{\mathbf{u}}_h^{n+1},\mathrm{div}\mathbf{v}_h\right),\end{aligned}\tag{3.6}$$

where $0<\varepsilon\leq 1$ is a penalty parameter.

Step IV: According to Step II and Step III, we get $\hat{\mathbf{u}}_h^{n+1}\in\mathbf{X}_h$ and find $p_h^{n+1}\in M_h$ by

$$\hat{\mathbf{u}}_h^{n+1}=\tilde{\mathbf{u}}_h^{n+1}+\bar{\mathbf{u}}_h^{n+1},\tag{3.7a}$$

$$(p_h^{n+1},q_h)=(D(p_h^n),q_h)-\frac{1}{\varepsilon}(\mathrm{div}\hat{\mathbf{u}}_h^{n+1},q_h),\quad\forall q_h\in M_h.\tag{3.7b}$$

Step V: Implement Step IV of Algorithm 3.1 with

$$\gamma^{n+1}=1-\left(1-\frac{Q^{n+1}}{E(\hat{\mathbf{u}}_h^{n+1},\tilde{\mathbf{H}}_h^{n+1})+C_0}\right)^3.$$

Remark 3.2. The projection method imposes artificial Neumann boundary condition for pressure and sacrifices pressure accuracy to decouple the velocity field and pressure. For Algorithms 3.1 and 3.2, the VPP$_\varepsilon$ technique is used to decouple the velocity and pressure. Further, compared to the projection method, the numerical experiments in Section 4.1 indicate that Algorithm 3.2 keeps second-order temporal accuracy for the velocity field and pressure in H^1 semi-norm and L^2 norm, respectively.

Remark 3.3. The velocity correction steps (3.2)-(3.3b) for the first-order scheme and (3.6)-(3.7b) for the second-order scheme perform an approximate divergence-free projection, and can get control of mass conservation law for the discrete solution when the penalty parameter is small.

In the following context, we mainly prove the stability of Algorithms 3.1 and 3.2. To the best of the authors' knowledge, it is the first work which obtains the stability of the fully discrete VPP$_\varepsilon$ scheme.

The proof for two algorithms is almost the same, so we shall only consider Algorithm 3.1. Additionally, the proof of stability for Algorithm 3.2 will be interspersed in following context by a concise format.

Theorem 3.1. *Suppose that*

$$\|\mathbf{f}(\cdot,t)\|_0\leq C_f,\quad\sigma^{-1}\mu^{-\frac{1}{2}}\|\mathrm{curl}\mathbf{g}(\cdot,t)\|_0\leq C_g$$

for all $t\in(0,T]$, *and* $\{\mathbf{u}_h^{n+1}\}$ *and* $\{\mathbf{H}_h^{n+1}\}$ *are the solutions to Algorithms* 3.1 *and* 3.2. *If* $C_0\geq \max\{\lambda C_f^2,\lambda C_g^2,1\}$ *with* $1\leq\lambda<\infty$, *and* $\Delta t<\sqrt{0.5\lambda}$, *then we have* $Q^{n+1}>0$. *Besides, there exists a constant* M_T *only dependent on* T *such that*

$$\|\mathbf{u}_h^{n+1}\|_0+\sqrt{\mu}\|\mathbf{H}_h^{n+1}\|_0\leq M_T,\quad \forall n\leq N-1. \tag{3.8}$$

In addition, for Algorithms 3.1 *and* 3.2, *there exist some positive constants* C_1, C_2, C_3, C_4 *independent on* h, Δt, ε, *such that*

$$Q^N+\Delta t\sum_{n=0}^{N-1}\frac{Q^{n+1}}{E(\hat{\mathbf{u}}_h^{n+1},\tilde{\mathbf{H}}_h^{n+1})+C_0}\left(\nu\|\nabla\hat{\mathbf{u}}_h^{n+1}\|_0^2+\sigma^{-1}\|\mathrm{curl}\tilde{\mathbf{H}}_h^{n+1}\|_0^2\right)\leq C_1, \tag{3.9a}$$

$$\varepsilon^2\sum_{n=0}^{N-1}\|\bar{\mathbf{u}}_h^{n+1}\|_0^2+\frac{\varepsilon^2\nu\Delta t}{2}\sum_{n=0}^{N-1}\|\nabla\bar{\mathbf{u}}_h^{n+1}\|_0^2\leq C_2\quad \textit{for Algorithm } 3.1, \tag{3.9b}$$

$$\varepsilon^2\|\bar{\mathbf{u}}_h^{N}\|_0^2+\varepsilon^2\nu\Delta t\sum_{n=1}^{N-1}\|\nabla\bar{\mathbf{u}}_h^{n+1}\|_0^2\leq C_3\qquad \textit{for Algorithm } 3.2, \tag{3.9c}$$

$$\nu\Delta t\sum_{n=0}^{N-1}\|\nabla\tilde{\mathbf{u}}_h^{n+1}\|_0^2\leq C_4. \tag{3.9d}$$

Remark 3.4. If we choose the big value of C_0, then λ will be big which weakens the time step restriction.

Proof. By the assumptions on $\mathbf{f}$, $\mathbf{g}$ and C_0, we have the following bounds with help of the Cauchy-Schwarz inequality

$$\frac{\left(\mathbf{f}^{n+1},\hat{\mathbf{u}}_h^{n+1}\right)}{E(\hat{\mathbf{u}}_h^{n+1},\tilde{\mathbf{H}}_h^{n+1})+C_0}\leq\frac{\|\mathbf{f}^{n+1}\|_0\|\hat{\mathbf{u}}_h^{n+1}\|_0}{\frac{1}{2}\|\hat{\mathbf{u}}_h^{n+1}\|_0^2+\lambda\|\mathbf{f}^{n+1}\|_0^2}\leq\frac{1}{\sqrt{2\lambda}}, \tag{3.10a}$$

$$\frac{\sigma^{-1}\left(\mathrm{curl}\mathbf{g}^{n+1},\tilde{\mathbf{H}}_h^{n+1}\right)}{E(\hat{\mathbf{u}}_h^{n+1},\tilde{\mathbf{H}}_h^{n+1})+C_0}\leq\frac{\sigma^{-1}\|\mathrm{curl}\mathbf{g}^{n+1}\|_0\|\tilde{\mathbf{H}}_h^{n+1}\|_0}{\frac{1}{2}\mu\|\tilde{\mathbf{H}}_h^{n+1}\|_0^2+\lambda\sigma^{-2}\mu^{-1}\|\mathrm{curl}\mathbf{g}^{n+1}\|_0^2}\leq\frac{1}{\sqrt{2\lambda}}, \tag{3.10b}$$

where we note that $a^2+b^2\geq 2ab$. In addition, according to (3.4a), we get

$$\begin{aligned}Q^{n+1}=&Q^n\Big(1+\frac{\Delta t}{E(\hat{\mathbf{u}}_h^{n+1},\tilde{\mathbf{H}}_h^{n+1})+C_0}\Big(\nu\|\nabla\hat{\mathbf{u}}_h^{n+1}\|_0^2+\sigma^{-1}\|\mathrm{curl}\tilde{\mathbf{H}}^{n+1}\|_0^2\\&-(\mathbf{f}^{n+1},\hat{\mathbf{u}}_h^{n+1})-\sigma^{-1}(\mathrm{curl}\mathbf{g}^{n+1},\tilde{\mathbf{H}}_h^{n+1})\Big)\Big)^{-1}\\=:&Q^n\left(1+\sum_{i=1}^4A_i\right)^{-1}.\end{aligned} \tag{3.11}$$

Next, we will prove $Q^n>0$, $0\leq n\leq N$ by using inductive method. First, we have $Q^0>0$. Second, assuming that $Q^{n-1}>0$, we will prove $Q^n>0$, $1\leq n\leq N$. In fact, it can be found

that $A_1, A_2 \geq 0$ in (3.11) and $A_3 + A_4 \geq -2\frac{\Delta t}{\sqrt{2\lambda}}$ from (3.10). Hence, if $\Delta t < \sqrt{0.5\lambda}$, then we obtain $1 + A_3 + A_4 > 0$ and $Q^n > 0$ from (3.11).

Moreover, taking the sum of (3.4a) for n from 0 to $N-1$ and applying (3.10), we obtain

$$\begin{aligned}
&Q^N + \Delta t \sum_{n=0}^{N-1} \frac{Q^{n+1}}{E(\hat{\mathbf{u}}_h^{n+1}, \tilde{\mathbf{H}}_h^{n+1}) + C_0} \left(\nu \|\nabla \hat{\mathbf{u}}_h^{n+1}\|_0^2 + \sigma^{-1} \|\mathrm{curl} \tilde{\mathbf{H}}_h^{n+1}\|_0^2 \right) \\
=&Q^0 + \Delta t \sum_{n=0}^{N-1} \frac{Q^{n+1}}{E(\hat{\mathbf{u}}_h^{n+1}, \tilde{\mathbf{H}}_h^{n+1}) + C_0} \left((\mathbf{f}^{n+1}, \tilde{\mathbf{u}}_h^{n+1}) + \sigma^{-1} (\mathrm{curl} \mathbf{g}^{n+1}, \tilde{\mathbf{H}}_h^{n+1}) \right) \\
\leq &Q^0 + \Delta t \sqrt{\frac{2}{\lambda}} \sum_{n=0}^{N-1} Q^{n+1}. \qquad (3.12)
\end{aligned}$$

Then, applying the discrete Grönwall lemma to (3.12), we have

$$\begin{aligned}
&Q^N + \Delta t \sum_{n=0}^{N-1} \frac{Q^{n+1}}{E(\hat{\mathbf{u}}_h^{n+1}, \tilde{\mathbf{H}}_h^{n+1}) + C_0} \left(\nu \|\nabla \hat{\mathbf{u}}_h^{n+1}\|_0^2 + \sigma^{-1} \|\mathrm{curl} \tilde{\mathbf{H}}_h^{n+1}\|_0^2 \right) \\
\leq &\exp\left(\sqrt{\frac{2}{\lambda}} T \right) Q^0,
\end{aligned}$$

which implies (3.9a). The above inequality along with $C_0 \geq 1$, we get

$$\frac{Q^{n+1}}{E(\hat{\mathbf{u}}_h^{n+1}, \tilde{\mathbf{H}}_h^{n+1}) + C_0} \leq \frac{2\exp\left(\sqrt{\frac{2}{\lambda}} T\right) Q^0}{\|\hat{\mathbf{u}}_h^{n+1}\|_0^2 + \mu \|\tilde{\mathbf{H}}_h^{n+1}\|_0^2 + 2}. \qquad (3.13)$$

Then, from (3.13), it is easy to show that there exists a constant $M_T > 0$ only dependent on T such that

$$\gamma^{n+1} \leq \frac{M_T}{\|\hat{\mathbf{u}}_h^{n+1}\|_0^2 + \mu \|\tilde{\mathbf{H}}_h^{n+1}\|_0^2 + 2},$$

which combines with

$$\mathbf{u}_h^{n+1} = \gamma^{n+1} \hat{\mathbf{u}}_h^{n+1} \quad \text{and} \quad \mathbf{H}_h^{n+1} = \gamma^{n+1} \tilde{\mathbf{H}}_h^{n+1}$$

to get

$$\begin{aligned}
&\|\mathbf{u}_h^{n+1}\|_0^2 = \left(\gamma^{n+1} \|\hat{\mathbf{u}}_h^{n+1}\|_0 \right)^2 \leq \frac{M_T^2}{\left(2\sqrt{2} \|\hat{\mathbf{u}}_h^{n+1}\|_0\right)^2} \|\hat{\mathbf{u}}_h^{n+1}\|_0^2 \leq M_T^2, \\
&\mu \|\mathbf{H}_h^{n+1}\|_0^2 \leq \mu \left(\gamma^{n+1} \|\tilde{\mathbf{H}}_h^{n+1}\|_0 \right)^2 \leq M_T^2,
\end{aligned}$$

which are (3.8).

Furthermore, for Algorithm 3.1, take $\mathbf{v}_h=\Delta t\bar{\mathbf{u}}_h^{n+1}$ in (3.2) and add the ensuing equation from $n=0$ to $N-1$, it follows from (3.3a) and the fact $\|\mathrm{div}\mathbf{v}\|_0\leq\|\nabla\mathbf{v}\|_0$ proved in [43] that

$$\begin{aligned}&\sum_{n=0}^{N-1}\|\bar{\mathbf{u}}_h^{n+1}\|_0^2+\nu\Delta t\sum_{n=0}^{N-1}\|\nabla\bar{\mathbf{u}}_h^{n+1}\|_0^2\\=&-\sum_{n=0}^{N-1}\frac{\Delta t}{\varepsilon}\left(\mathrm{div}\hat{\mathbf{u}}_h^{n+1},\mathrm{div}\bar{\mathbf{u}}_h^{n+1}\right)\\\leq&\frac{\nu\Delta t}{2}\sum_{n=0}^{N-1}\|\nabla\bar{\mathbf{u}}_h^{n+1}\|_0^2+\frac{\Delta t}{2\nu\varepsilon^2}\sum_{n=0}^{N-1}\|\nabla\hat{\mathbf{u}}_h^{n+1}\|_0^2,\end{aligned}\tag{3.14}$$

which, along with (3.9a) and (3.13), imply that there exists $C_2>0$ such that (3.9b) holds.

For Algorithm 3.2, choose $\mathbf{v}_h=4\Delta t\bar{\mathbf{u}}_h^{n+1}$ in (3.6) and add the ensuing equation from $n=1$ to $N-1$, it follows that

$$\begin{aligned}&\|\bar{\mathbf{u}}_h^N\|_0^2+\|2\bar{\mathbf{u}}_h^N-\bar{\mathbf{u}}_h^{N-1}\|_0^2+\sum_{n=1}^{N-1}\|\bar{\mathbf{u}}_h^{n+1}-2\bar{\mathbf{u}}_h^n+\bar{\mathbf{u}}_h^{n-1}\|_0^2+4\nu\Delta t\sum_{n=1}^{N-1}\|\nabla\bar{\mathbf{u}}_h^{n+1}\|_0^2\\=&-\sum_{n=0}^{N-1}\frac{4\Delta t}{\varepsilon}\left(\mathrm{div}\hat{\mathbf{u}}_h^{n+1},\mathrm{div}\bar{\mathbf{u}}_h^{n+1}\right)+\|\bar{\mathbf{u}}_h^1\|_0^2+\|2\bar{\mathbf{u}}_h^1-\bar{\mathbf{u}}_h^0\|_0^2\\\leq&3\nu\Delta t\sum_{n=1}^{N-1}\|\nabla\bar{\mathbf{u}}_h^{n+1}\|_0^2+\frac{4\Delta t}{3\nu\varepsilon^2}\sum_{n=1}^{N-1}\|\nabla\hat{\mathbf{u}}_h^{n+1}\|_0^2+\|\bar{\mathbf{u}}_h^1\|_0^2+\|2\bar{\mathbf{u}}_h^1-\bar{\mathbf{u}}_h^0\|_0^2,\end{aligned}$$

which combines (3.9a) and (3.9b) at $n=0$ to imply that there exists $C_3>0$ such that (3.9c) holds.

Finally, form (3.3a), we have

$$\Delta t\|\nabla\tilde{\mathbf{u}}_h^{n+1}\|_0^2\leq\Delta t\|\nabla\hat{\mathbf{u}}_h^{n+1}\|_0^2+2\Delta t\|\nabla\bar{\mathbf{u}}_h^{n+1}\|_0^2.$$

Then, from (3.9a) and (3.9b) (or (3.9c)), we derive that there exists $C_4>0$ such that (3.9d) holds. □

Corollary 3.1. *If* $\mathbf{f}=\mathbf{g}=\mathbf{0}$, *then we have* $0<Q^{n+1}<Q^n$, $\forall n\leq N-1$. *Besides, there exists a constant* M^* *independent on* T *such that*

$$\|\mathbf{u}_h^{n+1}\|_0+\sqrt{\mu}\|\mathbf{H}_h^{n+1}\|_0\leq M^*,\quad\forall n\leq N-1.\tag{3.15}$$

Proof. From (3.11), we obtain $Q^{n+1}>0$ by using inductive method. Then, according to (3.4a), we have

$$Q^{n+1}-Q^n=\frac{\Delta tQ^{n+1}}{E(\hat{\mathbf{u}}_h^{n+1},\tilde{\mathbf{H}}_h^{n+1})+C_0}\left(-\nu\|\nabla\hat{\mathbf{u}}_h^{n+1}\|_0^2-\sigma^{-1}\|\mathrm{curl}\tilde{\mathbf{H}}_h^{n+1}\|_0^2\right)<0.\tag{3.16}$$

By a similar argument of (3.8), we get (3.15). Unlike (3.8), note that the constant M^* here is independent on T. □

4 Numerical experiments

In this section, several numerical examples are tested to demonstrate the accuracy and efficiency of the proposed algorithms for the incompressible MHD model.

4.1 The MHD model with analytical solutions

4.1.1 2D convergence test

In order to verify the accuracy of the presented algorithms, the 2D incompressible MHD model (1.1a)-(1.2b) in the unit square domain $[0,1]^2$ is considered. The source terms and boundary conditions of the equations are determined by the analytic solution given below:

$$\begin{aligned}
&\mathbf{u}=(\alpha\pi\sin^2(\pi x)\sin(\pi y)\cos(\pi y)\cos(t),-\alpha\pi\sin(\pi x)\sin^2(\pi y)\cos(\pi x)\cos(t))^T,\\
&\mathbf{H}=(\alpha\sin(\pi x)\cos(\pi y)\cos(t),-\alpha\cos(\pi x)\sin(\pi y)\cos(t))^T,\\
&p=\alpha\cos(\pi x)\cos(\pi y)\cos(t),
\end{aligned}$$

where $\alpha=0.01$.

Firstly, we test the convergence order of Algorithm 3.1 with respect to h. Here we set $T=0.01$ and $\Delta t=0.001$. For the sake of simplicity, we denote the errors

$$err(s_h)=\|s_h^N-s_h^N\|_0,\quad s=\mathbf{u},p,\mathbf{H}\quad\text{and}\quad Err(\text{curl}\mathbf{H}_h)=\left((err(\mathbf{H}_h))^2+(err(\text{curl}\mathbf{H}_h))^2\right)^{\frac{1}{2}}.$$

Next, set the parameters $\nu=\mu=\sigma=\varepsilon=1.0$, $C_0=1000$ and pick five values of $h=\frac{1}{4}$, $\frac{1}{8}$, $\frac{1}{16}$, $\frac{1}{24}$ and $\frac{1}{32}$. Fig. 1(a) presents the errors of Algorithm 3.1. From the figure, we can see that the convergence orders with $err(\nabla\mathbf{u}_h)$, $err(p_h)$ and $Err(\text{curl}\mathbf{H}_h)$ are $\mathcal{O}(h)$, and the convergence order with $err(\mathbf{u}_h)$ is $\mathcal{O}(h^2)$.

Secondly, we fix $h=\frac{1}{24}$, $T=1$, $\varepsilon=1.0E-3$ and choose the same physics parameters as the above test to test the temporal accuracy. Take $\Delta t=\frac{1}{8}$, $\frac{1}{16}$, $\frac{1}{32}$, $\frac{1}{64}$, $\frac{1}{128}$, and denote the error with respect to the time step by

$$err(s_h^{\Delta t})=\|s_h^{N,\Delta t}-s_h^{N,\frac{\Delta t}{2}}\|_0\quad\text{and}\quad Err(\text{curl}\mathbf{H}_h^{\Delta t})=\left((err(\mathbf{H}_h^{\Delta t}))^2+(err(\text{curl}\mathbf{H}_h^{\Delta t}))^2\right)^{\frac{1}{2}}.$$

The errors and convergence rates of Algorithms 3.1 and 3.2 with respect to Δt are shown in Figs. 1(b) and (c), respectively. Both of them are approximately 1 or 2, which are the optimal order for first-order time discretization and second-order time discretization.

4.1.2 3D convergence test

In this numerical example, the temporal-spatial accuracy for the 3D incompressible MHD model is tested with the computational domain $\Omega=[0,1]^3$. Consider the problem (1.1a)-

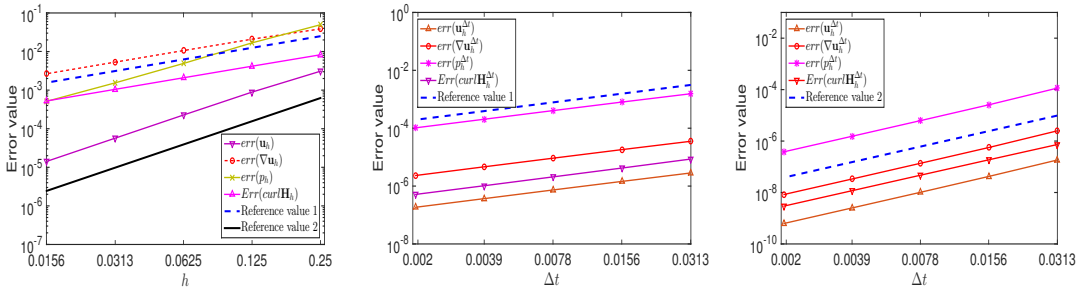

(a) (b) (c)

Figure 1: Errors and convergence rates with respect to h (a), Δt with first-order accuracy (b) and second-order accuracy (c).

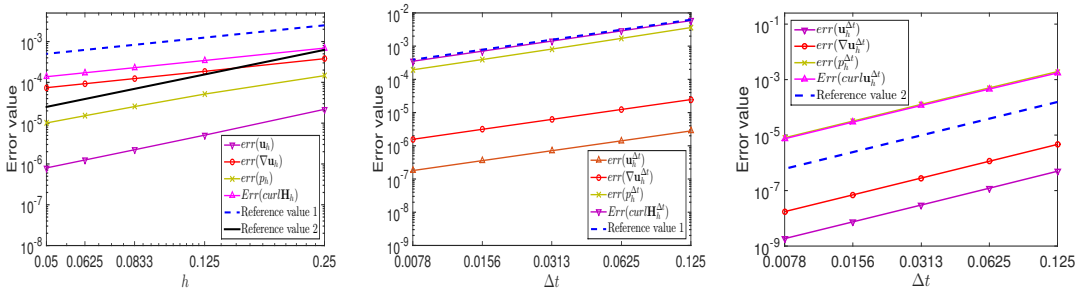

(a) (b) (c)

Figure 2: Errors and convergence rates with respect to h (a), Δt with first-order accuracy (b) and second-order accuracy (c).

(1.2b) with the following analytic solution

$$\mathbf{u}=(y^2z^2\sin(t),x^2z^2\sin(t),x^2y^2\sin(t))^T,\quad p=(1-x)(1-y)(1-z)\sin(t),$$
$$\mathbf{H}=(y(1-y)^2z(1-z)^2\sin(t),x(1-x)^2z(1-z)^2\sin(t),x(1-x)^2y(1-y)^2\sin(t))^T.$$

The functions $\mathbf{f}$ and $\mathbf{g}$ are obliged to satisfy that $\mathbf{u}$, p and $\mathbf{H}$ are the solutions of the original problem, respectively. Choose the same physics parameters as those in the 2D convergence test.

The errors and convergence rates with respect to h for Algorithm 3.1 are displayed in Fig. 2(a). Next, in order to test the temporal accuracy of Algorithms 3.1 and 3.2, the spatial step is fixed as $h=\frac{1}{12}$. The errors and convergence rates are shown in Figs. 2(b) and (c), from which we can see that Algorithms 3.1 and 3.2 work well and keep the convergence rates.

4.2 Hartmann flow

Hartmann flow, which describes the internal flow of a liquid metal through a channel under the influence of a transverse magnetic field $\mathbf{H}^d$, is a benchmark problem extensively implemented to test the MHD model (1.1a)-(1.2b). In this test, we consider the 2D/3D Hartmann flow with four physical parameters: fluid Reynolds number R_e, magnetic Reynolds number R_m, coupling coefficient s and Hartmann number H_a. The relationship between these parameters and the parameters in the model (1.1a)-(1.2b) is showed as follows

$$R_e=\nu^{-1},\quad R_m=\mu\sigma,\quad s=\mu^{-1},\quad H_a=\sqrt{R_eR_ms}.$$

4.2.1 2D Hartmann flow

The incompressible flow under an external transverse magnetic field $\mathbf{H}^2=(0,1)^T$ in a given domain $\Omega=[0,2]\times[-1,1]$ is considered in this test. The exact solution for the 2D incompressible MHD model (1.1a)-(1.2b) is provided [18].

$$\mathbf{u}(x,y)=(u(y),0)^T,\quad \mathbf{H}(x,y)=(H(y),1)^T,\quad p(x,y)=-x-sH^2(y)/2+10,$$

with

$$u(y)=\frac{R_e}{H_a\tanh(H_a)}\left(1-\frac{\cosh(yH_a)}{\cosh(H_a)}\right)\quad\text{and}\quad H(y)=\frac{1}{s}\left(\frac{\sinh(yH_a)}{\sinh(H_a)}-y\right).$$

The boundary conditions are chosen as no-slip boundary conditions on the wall and Neumann boundary conditions on the inlet and the outlet:

$$\mathbf{u}=0\quad\text{on } y=\pm1,\quad (p\mathbf{I}-R_e^{-1}\nabla\mathbf{u})\mathbf{n}=p\mathbf{n}\quad\text{on } x=0\quad\text{and}\quad x=2,\quad \mathbf{n}\times\mathbf{H}=\mathbf{n}\times\mathbf{H}^2\quad\text{on }\partial\Omega,$$

where $\mathbf{I}$ is identity matrix.

Set $C_0=1000$, $\varepsilon=1.0$, $\Delta t=\frac{1}{100}$, $h=\frac{1}{60}$ and $T=5$. Besides, we select the following three sets of physical parameters:

Case 1: $H_a=0.5$, $_e=R_m=0.1$, $s=25$;

Case 2: $H_a=5$, $R_e=R_m=1$, $s=25$;

Case 3: $H_a=50$, $R_e=R_m=10$, $s=25$.

The numerical results obtained by Algorithm 3.1 and the analytical solutions of the first components $u(y)$ and $H(y)$ are shown in Fig. 3, which suggests that the numerical results are in good agreement with the analytical solutions.

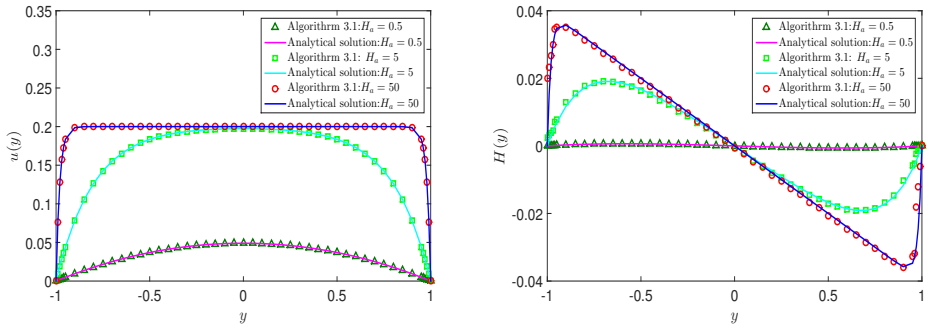

Figure 3: Slices of the 2D Hartmann flow at $x=1$, $-1\leq y\leq 1$.

4.2.2 3D Hartmann flow

A 3D unidirectional flow under an external transverse magnetic field $\mathbf{H}^3=(0,1,0)^T$ in a given domain $\Omega=[0,x_0]\times[-y_0,y_0]\times[-z_0,z_0]$ is considered in this test. The exact solution for the 3D Hartmann flow problem is provided as follows [18,40]:

$$\mathbf{u}(x,y,z)=(u(y,z),0,0)^T,\quad \mathbf{H}(x,y,z)=(H(y,z),1,0)^T,$$
$$p(x,y,z)=-x-sH^2(y,z)/2+10,$$

with

$$u(y,z)=\frac{1}{2}R_e\left(z^2-z_0^2\right)+\sum_{i=0}^{+\infty}a_i(y)\cosh(\lambda_i z),$$
$$H(y,z)=\sum_{i=0}^{+\infty}b_i(y)\cosh(\lambda_i z),$$

where

$$a_i(y)=A_i\cosh(p_1y)+B_i\cosh(p_2y),$$
$$b_i(y)=\frac{1}{R_es}\left(A_i\frac{\lambda_i^2-p_1^2}{p_1}\sinh(p_1y)+B_i\frac{\lambda_i^2-p_2^2}{p_2}\sinh(p_2y)\right).$$

Here

$$A_i=\frac{p_1(p_2^2-\lambda_i^2)}{\gamma_i}u_i(y_0)\sinh(p_2y_0),\quad B_i=\frac{p_2(\lambda_i^2-p_1^2)}{\gamma_i}u_i(y_0)\sinh(p_2y_0),$$
$$p_{1,2}^2=\lambda_i^2+\frac{H_a^2}{2}\pm H_a\sqrt{\lambda_i^2+\frac{H_a^2}{4}},\quad \lambda_i=\frac{(2i+1)\pi}{2z_0},$$
$$\gamma_i=p_2(\lambda_i^2-p_1^2)\sinh(p_1y_0)\cosh(p_2y_0)-p_1(\lambda_i^2-p_2^2)\sinh(p_2y_0)\cosh(p_1y_0),$$
$$u_i(y_0)=\frac{-2R_e}{\lambda_i^3z_0}\sin(\lambda_iz_0).$$

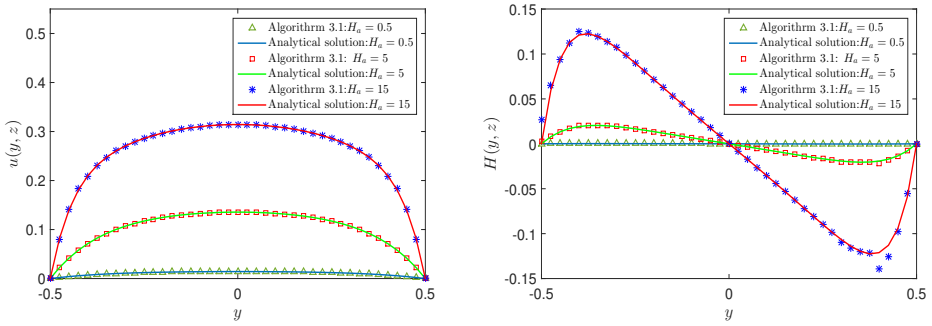

Figure 4: Slices of the 3D Hartmann flow at $x=1$, $-1\le y\le 1$, and $z=0$.

The following boundary conditions are imposed

$$\mathbf{u}=0 \quad \text{on } y=\pm y_0, \quad z=\pm z_0, \quad (p\mathbf{I}-R_e^{-1}\nabla\mathbf{u})\mathbf{n}=p\mathbf{n} \quad \text{on } x=0 \quad \text{and} \quad x=2,$$
$$\mathbf{n}\times\mathbf{H}=\mathbf{n}\times\mathbf{H}^3 \quad \text{on } \partial\Omega.$$

We choose the same values of C_0 and ε as those of the 2D Hartmann flow, and set $x_0=2$, $y_0=\frac{1}{2}$, $z_0=\frac{1}{4}$ and $\mathbf{f}=\mathbf{g}=0$. Take $T=3$, $\Delta t=\frac{1}{12}$ and $h=\frac{1}{10}$. Next, consider the following three cases:

Case 1: $H_a=0.5$, $R_e=R_m=0.5$, $s=1$;

Case 2: $H_a=5$, $R_e=R_m=5$, $s=1$;

Case 3: $H_a=15$, $R_e=R_m=15$, $s=1$.

The numerical results obtained by Algorithm 3.1 and the analytical solutions of $u(y,z)$ and $H(y,z)$ are presented in Fig. 4. We can see easily from the figure that the computational numerical points lie on the theoretical lines accordingly, which show that there exists a good agreement between the computational solutions and the analytical solutions.

4.3 Stability test

In order to test the stability of Algorithm 3.2, we consider the domain of the model (1.1a)-(1.2b) as the unit square $[0,1]^2$. Meanwhile, we compare Algorithm 3.2 with the following algorithm, which is the implicit/explicit scheme with second-order temporal accuracy.

Algorithm 4.1. Given $\mathbf{u}_h^n,\mathbf{u}_h^{n-1}\in\mathbf{X}_h$, $\mathbf{H}_h^n,\mathbf{H}_h^{n-1}\in\mathbf{W}_h$, find $(\mathbf{u}_h^{n+1},p_h^{n+1},\mathbf{H}_h^{n+1})\in\mathbf{X}_h\times M_h\times\mathbf{W}_h$

satisfying for all $(\mathbf{v}_h, q_h, \mathbf{B}_h) \in \mathbf{X}_h \times M_h \times \mathbf{W}_h$,

$$\left(\frac{3\mathbf{u}_h^{n+1}-4\mathbf{u}_h^n+\mathbf{u}_h^{n-1}}{2\Delta t},\mathbf{v}_h\right)+\nu(\nabla\mathbf{u}_h^{n+1},\nabla\mathbf{v}_h)+\Big((\mathbf{D}(\mathbf{u}_h^n)\cdot\nabla)\mathbf{D}(\mathbf{u}_h^n),\mathbf{v}_h\Big)$$
$$+\mu\Big(\mathbf{D}(\mathbf{H}_h^n)\times\mathrm{curl}\mathbf{D}(\mathbf{H}_h^n),\mathbf{v}_h\Big)-(\mathrm{div}\mathbf{v}_h,p_h^{n+1})+(\mathrm{div}\mathbf{u}_h^{n+1},q_h)=(\mathbf{f}^{n+1},\mathbf{v}_h), \tag{4.1a}$$
$$\mu\left(\frac{3\mathbf{H}_h^{n+1}-4\mathbf{H}_h^n+\mathbf{H}_h^{n-1}}{2\Delta t},\mathbf{B}_h\right)+\sigma^{-1}(\mathrm{curl}\mathbf{H}_h^{n+1},\mathrm{curl}\mathbf{B}_h)-\mu\Big(\mathrm{curl}\mathbf{D}(\mathbf{H}_h^n)\times\mathbf{B}_h,\mathbf{D}(\mathbf{u}_h^n)\Big)$$
$$=\sigma^{-1}(\mathrm{curl}\mathbf{g}^{n+1},\mathbf{B}_h). \tag{4.1b}$$

The source functions $\mathbf{f}$, $\mathbf{g}$ are set to zero. The initial values are taken as follows:

Case I: $\mathbf{u}_0(x,y)=(10x^2(x-1)^2y(y-1)(2y-1),-10y^2(y-1)^2x(x-1)(2x-1))^T$,
$\mathbf{H}_0(x,y)=(\sin(\pi x)\cos(\pi y),-\sin(\pi y)\cos(\pi x))^T$, $p_0(x,y)=0$.

Case II: $\mathbf{u}_0(x,y)=(y^2,x^2)^T$, $p_0(x,y)=(2x-1)(2y-1)$,
$\mathbf{H}_0(x,y)=(x^2(x-1)^2y(y-1)(2y-1),-y^2(y-1)^2x(x-1)(2x-1))^T$.

Here, for Case I, we take the physical parameters $\nu^{-1}=\sigma=100$, and vary $\Delta t=0.5$, 0.2, 0.1, 0.05. For Case II, we take the physical parameters $\nu^{-1}=1000$, $\sigma=100$, and vary $\Delta t=0.1$, 0.04, 0.02, 0.01. Moreover, we set $\varepsilon=1.0E-3$ and $T=10$. The discrete energy $E_h^n=\frac{1}{2}(\|\mathbf{u}_h^n\|_0^2+\mu\|\mathbf{H}_h^n\|_0^2)$ will be computed by Algorithms 3.2 and 4.1. The results of these two cases are displayed in Figs. 5 and 6, respectively. From Figs. 5(b) and 6(b), we observe that Algorithm 4.1 does not work when the large time steps are used. In contrast, from Figs. 5(a) and 6(a), the energy curves of Algorithm 3.2 shows monotonic decay for all the tested time steps, which is not surprising since Algorithm 3.2 is stable from Theorem 3.1.

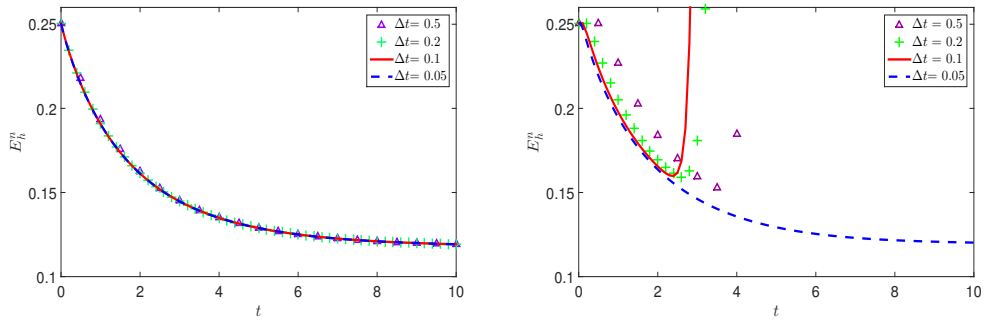

(a) (b)

Figure 5: The value E_h^n of Algorithm 3.2 (a) and Algorithm 4.1 (b) with different time steps for Case I.

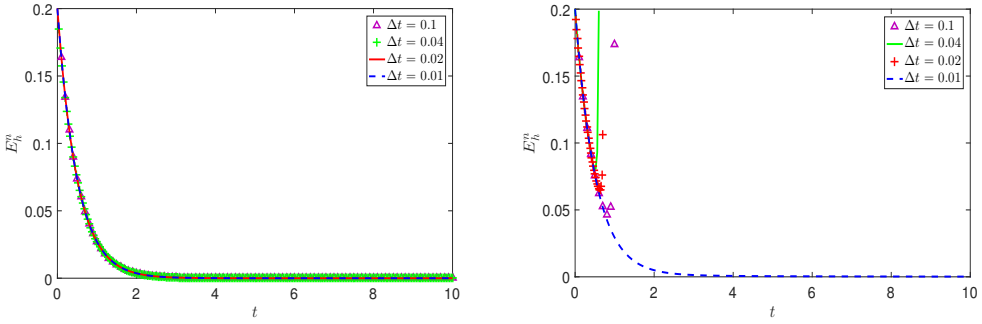

(a) (b)

Figure 6: The value E_h^n of Algorithm 3.2 (a) and Algorithm 4.1 (b) with different time steps for Case II.

4.4 An exact solution problem

In order to demonstrate the effectiveness of Algorithm 3.2 discussed in this paper, we will test the numerical example in [61]. Consider the MHD model in the unit domain $[0,1]^2$ and the time interval $[0,1]$. The source terms $\mathbf{f}$ and $\mathbf{g}$, initial and boundary conditions are chosen to ensure that

$$\mathbf{u} = (t^4\sin^2(k\pi x)\sin(2k\pi y), -t^4\sin^2(k\pi y)\sin(2k\pi x))^T,$$
$$\mathbf{H} = (-\sin(ky)t^4, \sin(kx)t^4)^T, \quad p = t^4\cos(\pi x)\cos(\pi y),$$

is the solution to the problem (1.1a)-(1.2b).

Taking $\nu = \sigma = \mu = 1$, $k = 0.1$, $\varepsilon = 0.1$, $C_0 = 1000$ and fixing the spatial mesh size $h = \frac{1}{300}$, we list the numerical results of Algorithm 3.2 in Table 1, from which we find that it has better error than that in [61].

Next, we consider the choice of the parameter C_0. Note that in Theorem 3.1 we need $\Delta t < \sqrt{0.5\lambda}$ and $C_0 \geq \max\{\lambda C_f^2, \lambda C_g^2, 1\}$. If we choose the big value of C_0, then λ will be big which weakens this time step restriction. If we fix the time step Δt, then $\lambda > 2(\Delta t)^2$ and $C_0 \geq \max\{2(\Delta t)^2 C_f^2, 2(\Delta t)^2 C_g^2, 1\}$. Hence, if we choose small value of C_0, then Algorithm 3.2 will do not work.

Table 1: The errors and divergence of velocity with different time steps.

	Algorithm 3.2				error in [61]
Δt	$err(\mathbf{u}_h)$	$err(\nabla\mathbf{u}_h)$	$err(p_h)$	$\|\mathrm{div}\mathbf{u}_h\|_0$	$err(\mathbf{u}_h)$
$\frac{1}{10}$	$1.21E{-}3$	$9.10E{-}3$	$1.85E{-}2$	$4.83E{-}3$	$1.00E{-}2$
$\frac{1}{20}$	$3.38E{-}4$	$2.56E{-}3$	$5.18E{-}3$	$1.37E{-}3$	$4.87E{-}3$
$\frac{1}{40}$	$8.92E{-}5$	$7.07E{-}4$	$1.37E{-}3$	$4.08E{-}4$	$1.58E{-}3$
$\frac{1}{80}$	$2.29E{-}5$	$2.79E{-}4$	$3.82E{-}4$	$2.19E{-}4$	$4.30E{-}4$

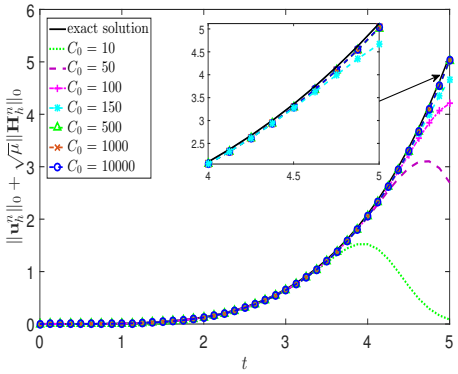

Figure 7: The value of $\|\mathbf{u}_h^n\|_0+\sqrt{\mu}\|\mathbf{H}_h^n\|_0$ by Algorithm 3.2 with different C_0.

Fix $\nu=\sigma=\mu=1$, $k=0.01$, $\varepsilon=0.001$ and $h=\Delta t=\frac{1}{48}$ to show the evolution of the values of $\|\mathbf{u}_h^n\|_0+\sqrt{\mu}\|\mathbf{H}_h^n\|_0$ and $1-\gamma^n$ $(1\le n\le N)$ obtained by Algorithm 3.2. Obviously, we can see from Fig. 7 that Algorithm 3.2 with the small value of C_0 does not work, and the curves are gradually decreasing after $t=4$, which are opposite to the exact solution. However, the numerical result with the big value of C_0 is agreement with the exact solution. Furthermore, we show the values of $1-\gamma^N$ and $\|\mathbf{u}_h^N\|_0+\sqrt{\mu}\|\mathbf{H}_h^N\|_0$ (denoted as $\mathbb{E}^N$) by Algorithm 3.2 in Table 2 with different C_0, which imply that Algorithm 3.2 with big value of C_0 produces better numerical results than those of Algorithm 3.2 with small value of C_0.

Finally, by varying the value of ε, we test the influence of ε on the numerical results for Algorithm 3.2 with $\Delta t=h=\frac{1}{24}$. The numerical results are showed in Table 3. It is found that, as ε gradually decreases, the errors decrease.

Table 2: The numerical results of Algorithm 3.2 at $T=5$.

C_0	10	50	100	150	500	1000	10000	exact solution
$\mathbb{E}^N$	0.08487	2.6981	4.2081	4.6666	5.0140	5.0298	5.0324	5.1172
$1-\gamma^N$	9.85E−1	4.84E−1	1.75E−1	7.88E−2	4.06E−3	5.89E−4	6.76E−7	—

Table 3: The errors of the velocity with $k=0.001$ by Algorithm 3.2 under different values of ε.

ε	1.0	$1.0E-1$	$1.0E-2$	$1.0E-3$	$1.0E-4$	$1.0E-5$
$\|\mathrm{div}\mathbf{u}_h^N\|_0$	$9.69E-3$	$9.81E-4$	$9.82E-5$	$9.82E-6$	$9.82E-7$	$9.82E-8$
$err(\mathbf{u}_h)$	$2.37E-3$	$2.39E-4$	$2.37E-5$	$2.35E-6$	$2.35E-7$	$2.35E-8$
$err(\nabla\mathbf{u}_h)$	$1.80E-2$	$1.83E-3$	$1.84E-4$	$1.87E-5$	$1.88E-6$	$1.88E-7$

4.5 Driven cavity flow

4.5.1 $2D$ driven cavity flow

In this subsection, the driven cavity flow problem is tested in a domain $\Omega=[0,1]^2$. Set $h=\frac{1}{64}$, $\Delta t=\frac{1}{100}$. Then, the source terms and initial values are set to zero. Impose the following boundary conditions:

$$\mathbf{u}=(0,0) \quad \text{on } x=0,1, \quad \text{and} \quad y=0, \quad \mathbf{u}=(1,0) \quad \text{on } y=1,$$
$$\mathbf{n}\times\mathbf{B}=\mathbf{n}\times\mathbf{B}_D \quad \text{on } \partial\Omega, \quad \text{where } \mathbf{B}_D=(1,0)^T.$$

The final time T is chosen such that

$$\|\mathbf{u}_h^N-\mathbf{u}_h^{N-1}\|_0+\|\mathbf{H}_h^N-\mathbf{H}_h^{N-1}\|_0\leq 1.0E-5.$$

Next, we plot the velocity streamline and magnetic obtained by Algorithm 3.2 with fixed $\nu=\sigma=1$, $\varepsilon=0.01$ and $\mu=1.0$ and 5.0 in Fig. 8. With the increase of μ, the magnetic field is starting to bend.

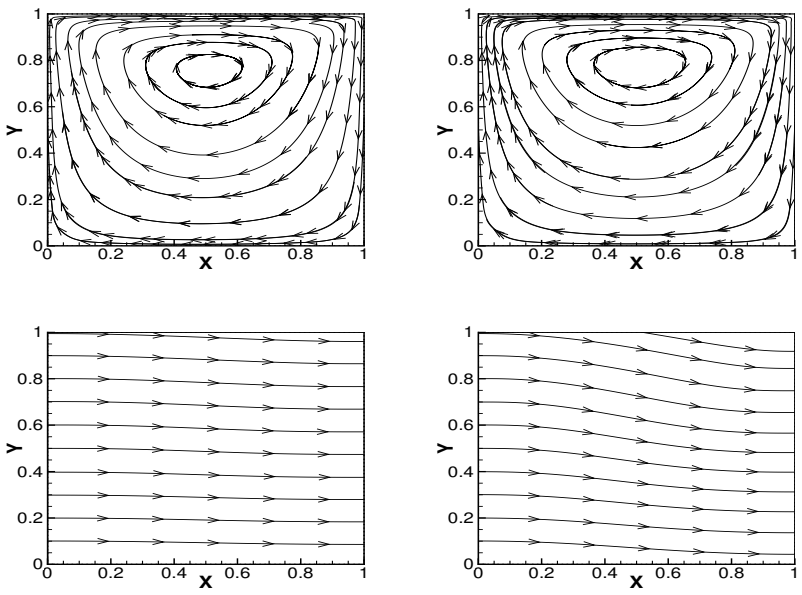

Figure 8: The streamlines of velocity field (the first line) and magnetic field (the second line) for $\mu=1.0$ (the first column) and $\mu=5.0$ (the second column).

4.5.2 3D driven cavity flow

In this example, let us consider the 3D MHD model in a driven cavity. The domain is defined in $\Omega=[0,1]^3$. Impose boundary conditions: $\mathbf{u}|_{S_T}=(w,0,0)^T$, $(\mathbf{H}\times\mathbf{n})|_{S_T}=\mathbf{H}_1\times\mathbf{n}$, where w satisfies $w(x,y,1)=1$ and $w(x,y,z)=0$ for $z\neq 1$, and $\mathbf{H}_1=(1,0,0)^T$.

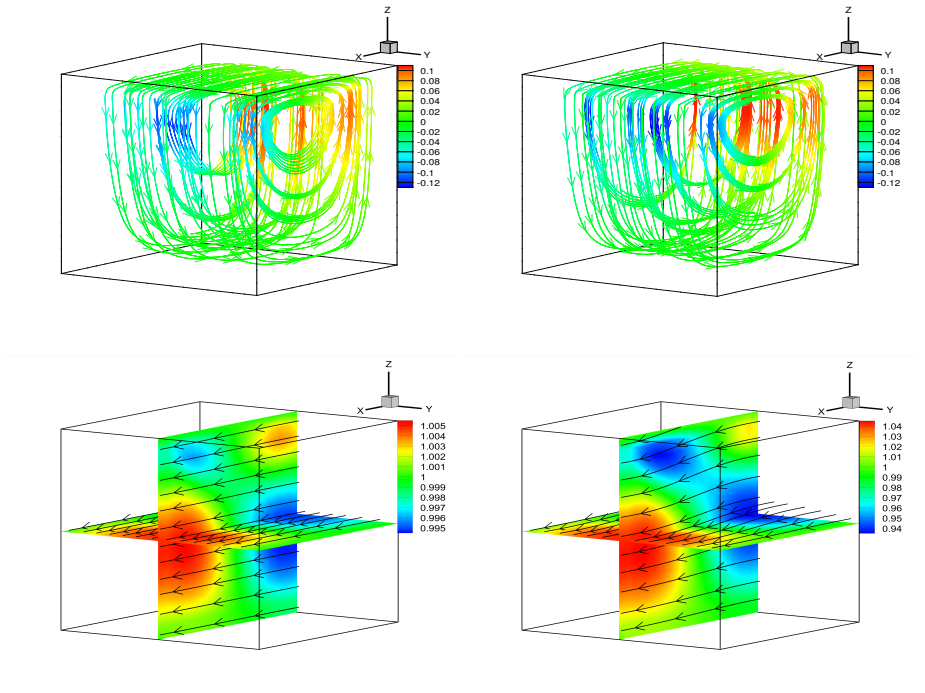

Figure 9: The streamlines of velocity field (the first line) and magnetic field (the second line) for $\mu=1.0$ (the first column) and $\mu=10.0$ (the second column).

We choose initial values $\mathbf{H}_0=(0,0,0)^T$, $\mathbf{u}_0=(0,0,0)^T$, test parameter $\nu=\sigma=1,\varepsilon=1.0E-3$ and set $\Delta t=0.01$, $h=\frac{1}{12}$. The final time T is chosen such that

$$\|\mathbf{u}_h^N-\mathbf{u}_h^{N-1}\|_0+\|\mathbf{H}_h^N-\mathbf{H}_h^{N-1}\|_0\leq 1.0E-5.$$

In this example, we mainly consider the effect of μ for the driven cavity flow problem solved by Algorithm 3.2. The numerical results of the velocity and magnetic fields are depicted in Fig. 9. As μ increases, the magnetic field is bent.

Acknowledgements

The authors would like to express their sincere gratitude to editor and anonymous reviewers for their helpful suggestions on the quality improvement of the present paper. This work is sponsored by the Natural Science Foundation of China (No. 12361077), Natural Science Foundation of Xinjiang Uygur Autonomous Region (No. 2023D14014) and Tianshan Talent Training Program of Xinjiang Uygur Autonomous Region (No. 2023TSYCCX0103).

References

[1] P. ANGOT, J. P. CALTAGIRONE, AND P. FABRIE, *Vector penalty-projection methods for the solution of unsteady incompressible flows*, in: R. Eymard, J.-M. Hérard (Eds.), Finite Volumes for Complex Applications V-Problems & Perspectives, ISTE Ltd., J. Wiley & Sons, (2008), pp. 169–176.

[2] P. ANGOT, J. P. CALTAGIRONE, AND P. FABRIE, *A fast vector penalty-projection method for incompressible non-homogeneous or multiphase Navier-Stokes problems,* Appl. Math. Lett., 25 (2012), pp. 1681–1688.

[3] P. ANGOT, J. P. CALTAGIRONE, AND P. FABRIE, *A kinematic vector penalty-projection method for incompressible flow with variable density,* C. R. Math., 354 (2016), pp. 1124–1131.

[4] X. ANTOINE, J. SHEN, AND Q. TANG, *Scalar auxiliary variable/Lagrange multiplier based pseudospectral schemes for the dynamics of nonlinear Schrödinger/Gross-Pitaevskii equations,* J. Comput. Phys., 437 (2021), 110328.

[5] D. N. ARNOLD, F. BREZZI, AND M. FORTIN, *A stable finite element for the Stokes equations,* Calcolo, 21 (1984), pp. 337–344.

[6] J. CARTER, D. Z. HAN, AND N. JIANG, *Second order, unconditionally stable, linear ensemble algorithms for the magnetohydrodynamics equations,* J. Sci. Comput., 94 (2023), 41.

[7] H. CHEN, Y. HE, AND H. CHEN, *Stability and temporal error estimate of scalar auxiliary variable schemes for the magnetohydrodynamics equations withvariable density,* Numer. Methods Part. Differ. Equs., 40 (2024), e23067.

[8] W. CHEN, K. L. WU, AND T. XIONG, *High order asymptotic preserving finite difference WENO schemes with constrained transport for MHD equations in all sonic Mach numbers,* J. Comput. Phys., 488 (2023), 112240.

[9] Q. CHENG, C. LIU, AND J. SHEN, *Generalized SAV approaches for gradient systems,* J. Comput. Appl. Math., 394 (2021), 113532.

[10] X. C. CHU, C. J. CHEN, AND T. ZHANG, *Stability and convergence of spatial discrete stabilized finite volume method for the unsteady incompressible magnetohydrodynamics equations,* Appl. Numer. Math., 181 (2022), pp. 436–467.

[11] A. ÇIBIK, F. G. EROGLU, AND S. KAYA, *Analysis of second order time filtered backward Euler method for MHD equations,* J. Sci. Comput., 82 (2020), pp. 1–25.

[12] W. L. DAI AND P. R. WOODWARD, *A simple finite difference scheme for multidimensional magnetohydrodynamical equations,* J. Comput. Phys., 142 (1998), pp. 331–369.

[13] P. A. DAVIDSON, An Introduction to Magnetohydrodynamics, Cambridge University Press, Cambridge, 2001.

[14] Y. N. DI, Y, H. MA, J. SHEN, AND J. W. ZHANG, *A variable time-step IMEX-BDF2 SAV scheme and its sharp error estimate for the Navier-Stokes equations,* ESAIM: Math. Model. Numer. Anal., 57 (2023), pp. 1143–1170.

[15] X. J. DONG AND Y. N. HE, *Optimal convergence analysis of Crank-Nicolson extrapolation scheme for the three-dimensional incompressible magnetohydrodynamics,* Comput. Math. Appl., 76 (2018), pp. 2678–2700.

[16] D. ERKMEN, S. K. MERDAN, AND A. ÇIBIK, *A second order decoupled penalty projection method based on deferred correction for MHD in Elässer variable,* J. Comput. Appl. Math., 371 (2020), 112694.

[17] H. GAO AND W. QIU, *A semi-implicit energy conserving finite element method for the dynamical incompressible magnetohydrodynamics equations,* Comput. Methods Appl. Mech. Eng., 346 (2019), pp. 982–1001.

[18] J. F. GERBEAU, C. L. BRIS, AND T. LELIÈVRE, Mathematical Methods for the Magnetohydrodynamics of Liquid Metals, Oxford University Press, Oxford, 2006.
[19] S. GHOSH, M. HOSSAIN, AND W. H. MATTHAEUS, *The application of spectral methods in simulating compressible fluid and magnetofluid turbulence,* Comput. Phys. Commun., 74 (1993), pp. 18–40.
[20] J. X. GUAN, S. J. JING, AND Z. Y. SI, *A rotational velocity-correction projection method for unsteady incompressible magnetohydrodynamics equations,* Comput. Math. Appl., 80 (2020), pp. 809–821.
[21] M. D. GUNZBURGER, O. A. LADYZHENSKAYA, AND J. S. PETERSON, *On the global unique solvability of initial boundary value problems for the coupled modified Navier-Stokes and Maxwell equations,* J. Math. Fluid Mech., 6 (2004), pp. 462–482.
[22] Y. N. HE, *Unconditional convergence of the Euler semi-implicit scheme for the 3D incompressible MHD equations,* IMA J. Numer. Anal., 35 (2015), pp. 767–801.
[23] J. HEYWOOD AND R. RANNACHER, *Finite element approximation of the nonstationary Navier-Stokes equations, IV: Error analysis for second order time discretizations,* SIAM J. Numer. Anal., 27 (1990), pp. 353–384.
[24] R. HIPTMAIR, L. LI, S. MAO, AND W. ZHENG, *A fully divergence-free finite element method for magnetohydrodynamic equations,* Math. Models Methods Appl. Sci., 28 (2018), pp. 659–695.
[25] P. Z. HUANG, *A finite element algorithm for the nonstationary incompressible magnetohydrodynamic system based on a correction method,* Mediterr. J. Math., 19 (2022), 113.
[26] F. K. HUANG AND J. SHEN, *Stability and error analysis of a class of high-order IMEX schemes for Navier–Stokes equations with periodic boundary conditions,* SIAM J. Numer. Anal., 59 (2021), pp. 2926–2954.
[27] F. K. HUANG AND J. SHEN, *A new class of implicit-explicit BDFk SAV schemes for general dissipative systems and their error analysis,* Comput. Methods Appl. Mech. Eng., 392 (2022), 114718.
[28] F. K. HUANG, J. SHEN, AND Z. G. YANG, *A highly efficient and accurate new scalar auxiliary variable approach for gradient flows,* SIAM J. Sci. Comput., 42 (2020), pp. A2514–A2536.
[29] M. S. JIANG, Z. Y. ZHANG, AND J. ZHAO, *Improving the accuracy and consistency of the scalar auxiliary variable (SAV) method with relaxation,* J. Comput. Phys., 456 (2022), 110954.
[30] X. L. LI AND J. SHEN, *On fully decoupled MSAV schemes for the Cahn-Hilliard-Navier-Stokes model of two-phase incompressible flows,* Math. Models Methods Appl. Sci., 32 (2022), pp. 457–495.
[31] X. L. LI AND J. SHEN, *Error estimate of a consistent splitting GSAV scheme for the Navier-Stokes equations,* Appl. Numer. Math., 188 (2023), pp. 62–74.
[32] X. L. LI, J. SHEN, AND Z. G. LIU, *New SAV-pressure correction methods for the Navier-Stokes equations: stability and error analysis,* Math. Comp., 91 (2021), pp. 141–167.
[33] X. L. LI, W. L. WANG, AND J. SHEN, *Stability and error analysis of IMEX SAV schemes for the magnetohydrodynamic equations,* SIAM J. Numer. Anal., 60 (2022), pp. 1026–1054.
[34] Y. LI AND C. ZHAI, *Unconditionally optimal convergence analysis of second-order BDF Galerkin finite element scheme for a hybrid MHD system,* Adv. Comput. Math., 46 (2020), 75.
[35] L. L. LIN, Z. G. YANG, AND S. C. DONG, *Numerical approximation of incompressible Navier-Stokes equations based on an auxiliary energy variable,* J. Comput. Phys., 388 (2019), pp. 1–22.
[36] S. J. LIU, P. Z. HUANG, AND Y. N. HE, *An optimal error estimate of the BDF-Galerkin FEM for the incompressible MHD system,* J. Math. Anal. Appl., 515 (2022), 126460.
[37] S. J. LIU, P. Z. HUANG, AND Y. N. HE, *A second-order scheme based on blended BDF for the incompressible MHD system,* Adv. Comput. Math., 49 (2023), pp. 1–25.
[38] J. G. LIU AND R. PEGO, *Stable discretization of magnetohydrodynamics in bounded domains,*

Commun. Math. Sci., 8 (2010), pp. 235–251.
[39] X. L. Lu, P. Z. Huang, and Y. N. He, *Fully discrete finite element approximation of the 2D/3D unsteady incompressible magnetohydrodynamic-Voigt regularization flows,* Discrete Contin. Dyn. Syst. Ser. B., 26 (2021), 815.
[40] X. L. Lu and P. Z. Huang, *A modular grad-div stabilization for the 2D/3D nonstationary incompressible magnetohydrodynamic equations,* J. Sci. Comput., 82 (2020), 3.
[41] H. M. Ma and P. Z. Huang, *A vector penalty-projection approach for the time-dependent incompressible magnetohydrodynamics flows,* Comput. Math. Appl., 120 (2022), pp. 28–44.
[42] R. Moreau, Magnetohydrodynamics, Kluwer Academic Publishers, Dordrecht, 1990.
[43] R. H. Nochetto and J. H. Pyo, *Optimal relaxation parameter for the Uzawa method,* Numer. Math., 98 (2004), pp. 695–702.
[44] A. Prohl, *Convergent finite element discretizations of the nonstationary incompressible magnetohydrodynamics system,* ESAIM: Math. Model. Numer. Anal., 42 (2008), pp. 1065–1087.
[45] F. Shakeri and D. Mehdi, *A finite volume spectral element method for solving magnetohydrodynamic (MHD) equations,* Appl. Numer. Math., 61 (2011), pp. 1–23.
[46] X. J. Shen, Y. X. Wang, and Z. Y. Si, *A rotational pressure-correction projection methods for unsteady incompressible magnetohydrodynamics equations,* Appl. Math. Comput., 387 (2020), 124488.
[47] J. Shen and J. Xu, *Convergence and error analysis for the scalar auxiliary variable (SAV) schemes to gradient flows,* SIAM J. Numer. Anal., 56 (2018), pp. 2895–2912.
[48] J. Shen, J. Xu, and J. Yang, *The scalar auxiliary variable (SAV) approach for gradient flows,* J. Comput. Phys., 353 (2018), pp. 407–416.
[49] J. Shen, J. Xu, and J. Yang, *A new class of efficient and robust energy stable schemes for gradient flows,* SIAM Rev., 61 (2019), pp. 474–506.
[50] W. L. Wang, *Novel pressure-correction schemes based on scalar auxiliary variable method for the MHD equations,* Appl. Math. Comput., 437 (2023), 127550.
[51] C. Wang, J. L. Wang, Z. Y. Xia, and L. W. Xu, *Optimal error estimates of a Crank-Nicolson finite element projection method for magnetohydrodynamic equations,* ESAIM: Math. Model. Numer. Anal., 56 (2022), pp. 767–789.
[52] K. Wang and G. D. Zhang, *Unconditionally energy stable, splitting schemes for magnetohydrodynamic equations,* Int. J. Numer. Methods Fluids, 93 (2021), pp. 1396–1418.
[53] K. Wu, F. K. Huang, and J. Shen, *A new class of higher-order decoupled schemes for the incompressible Navier-Stokes equations and applications to rotating dynamics,* J. Comput. Phys., 458 (2022), 111097.
[54] X. F. Yang, *Numerical approximations of the Navier-Stokes equation coupled with volume-conserved multi-phase-field vesicles system: Fully-decoupled, linear, unconditionally energy stable and second-order time-accurate numerical scheme,* Comput. Methods Appl. Mech. Engrg., 375 (2021), 113600.
[55] X. F. Yang, *A new efficient fully-decoupled and second-order time-accurate scheme for Cahn-Hilliard phase-field model of three-phase incompressible flow,* Comput. Methods Appl. Mech. Engrg., 376 (2021), 13589.
[56] X. F. Yang, *A novel fully decoupled scheme with second-order time accuracy and unconditional energy stability for the Navier-Stokes equations coupled with mass-conserved Allen-Cahn phase-field model of two-phase incompressible flow,* Int. J. Numer. Methods Eng., 122 (2021), pp. 1283–1306.
[57] X. F. Yang, *A novel fully-decoupled, second-order time-accurate, unconditionally energy stable scheme for a flow-coupled volume-conserved phase-field elastic bending energy model,* J. Comput. Phys., 432 (2021), 110015.

[58] X. F. YANG, *A novel fully-decoupled, second-order and energy stable numerical scheme of the conserved Allen-Cahn type flow-coupled binary surfactant model,* Comput. Methods Appl. Mech. Engrg., 373 (2021), 113502.
[59] J. J. YANG AND Y. N. HE, *Stability and error analysis for the first-order euler implicit/explicit scheme for the 3D MHD equations,* Int. J. Comput. Methods, 14 (2018), 1750077.
[60] J. J. YANG, Y. N. HE, AND G. D. ZHANG, *On an efficient second order backward difference Newton scheme for MHD system,* J. Math. Anal. Appl., 458 (2018), pp. 676–714.
[61] J. J. YANG AND S. P. MAO, *Second order fully decoupled and unconditionally energy-stable finite element algorithm for the incompressible MHD equations,* Appl. Math. Lett., 121 (2021), 107467.
[62] X. F. YANG, G. D. ZHANG, AND X. M. HE, *Convergence analysis of an unconditionally energy stable projection scheme for magneto-hydrodynamic equations,* Appl. Numer. Math., 136 (2019), pp. 235–256.
[63] G. D. ZHANG AND Y. N. HE, *Unconditional convergence of the Euler semi-implicit scheme for the 3D incompressible MHD equations,* Numerical implementation, Int. J. Numer. Meth. Heat Fluid Flow., 25 (2015), pp. 1912–1923.
[64] G. D. ZHANG AND Y. N. HE, *Decoupled schemes for unsteady MHD equations II: Finite element discretization and numerical implementation,* Comput. Math. Appl., 69 (2015), pp. 1390–1406.
[65] G. D. ZHANG AND Y N. HE, *Decoupled schemes for unsteady MHD equations. I. Time discretization,* Numer. Meth. Part. Differ. Equs., 33 (2017), pp. 956–973.
[66] G. D. ZHANG, X. M. HE, AND X. F. YANG, *A decoupled, linear and unconditionally energy stable scheme with finite element discretizations for magnetohydrodynamic equations,* J. Sci. Comput., 81 (2019), pp. 167–1711.
[67] G. D. ZHANG, X. M. HE, AND X. F. YANG, *Fully decoupled, linear and unconditionally energy stable time discretization scheme for solving the magneto-hydrodynamic equations,* J. Comput. Appl. Math., 369 (2020), 112636.
[68] G. D. ZHANG, X. M. HE, AND X. F. YANG, *A fully decoupled linearized finite element method with second-order temporal accuracy and unconditional energy stability for incompressible MHD equations,* J. Comput. Phys., (2021), 110752.
[69] Y. H. ZHANG, Y. R. HOU, AND L. SHAN, *Numerical analysis of the Crank-Nicolson extrapolation time discrete scheme for magnetohydrodynamics flows,* Numer. Meth. Part. Differ. Equs., 31 (2015), pp. 2169–2208.
[70] Y. R. ZHANG AND J. SHEN, *A generalized SAV approach with relaxation for dissipative systems,* J. Comput. Phys., 464 (2022), 111311.
[71] Q. ZHANG, H. Y. SU, AND X. L. FENG, *A partitioned finite element scheme based on Gauge-Uzawa method for time-dependent MHD equations,* Numer. Algor., 78 (2018), pp. 277–295.
[72] K. ZHANG, H. Y. SU, AND D. M. LIU, *2D/3D fully decoupled, unconditionally energy stable rotational velocity projection method for incompressible MHD System,* J. Math. Fluid Mech., 25 (2023), pp. 1–14.
[73] T. ZHANG AND J. T. YANG, *Decoupled and linearized scalar auxiliary variable finite element method for the time-dependent incompressible magnetohydrodynamic equations: Unconditional stability and convergence analysis,* Numer. Meth. Part. Differ. Equs., 38 (2022), pp. 1499–1525.
[74] G. D. ZHANG, J. J. YANG AND C. J. BI, *Second order unconditionally convergent and energy stable linearized scheme for MHD equations,* Adv. Comput. Math., 44 (2018), pp. 505–540.
[75] T. ZHANG AND J. Y. YUAN, *Unconditional stability and optimal error estimates of Euler implicit/explicit-SAV scheme for the Navier-Stokes equations,* J. Sci. Comput., 90 (2022), pp. 1–20.